Inside the Alloy Mechanism of Sb and Bi Electrodes for K-ion Batteries

Vincent Gabaudan [ab], Romain Berthelot [ab], Lorenzo Stievano [ab], Laure Monconduit*[ab]

[a]*ICGM, Université de Montpellier, CNRS, Montpellier, France*

[a]*Réseau sur le Stockage Electrochimique de l'Energie (RS2E), FR CNRS 3459, France*

SUPPLEMENTARY INFORMATION:

Cyclic voltammetry

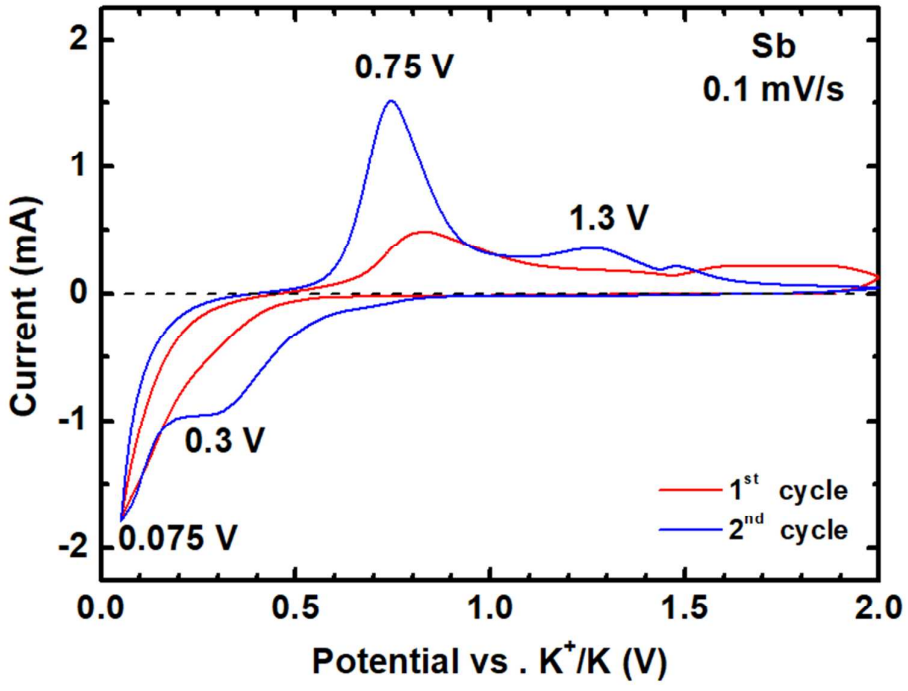

Figure S1. Cyclic voltammogram of Sb half-cell for the first two cycles at a scan rate of 0.1 mV/s between 0.05 and 2.0 V

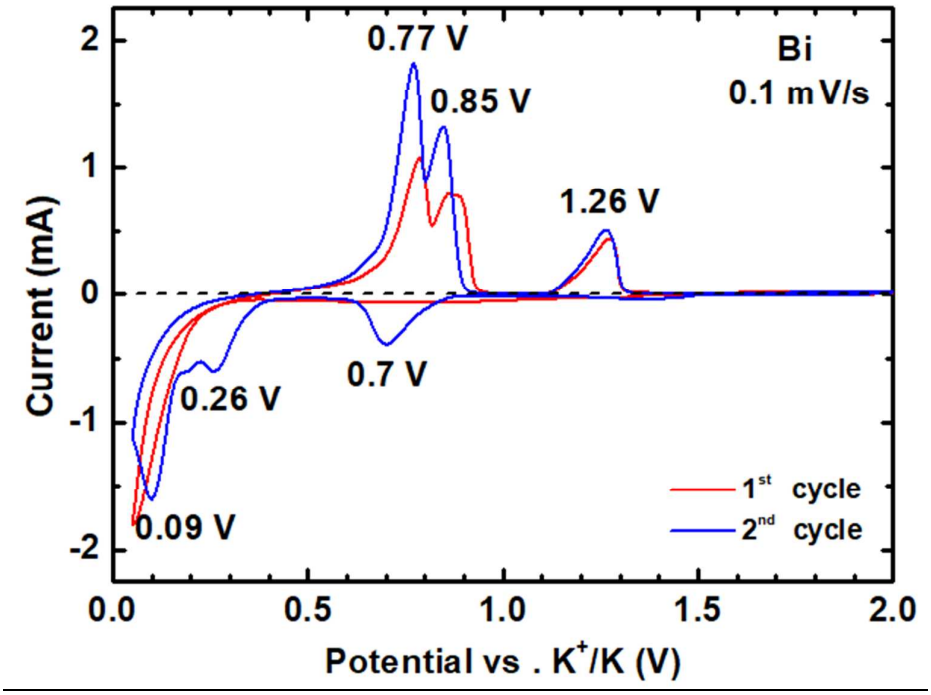

Figure S2. Cyclic voltammogram of Bi half-cell for the first two cycles at a scan rate of 0.1 mV/s between 0.05 and 2.0 V

Phase diagram

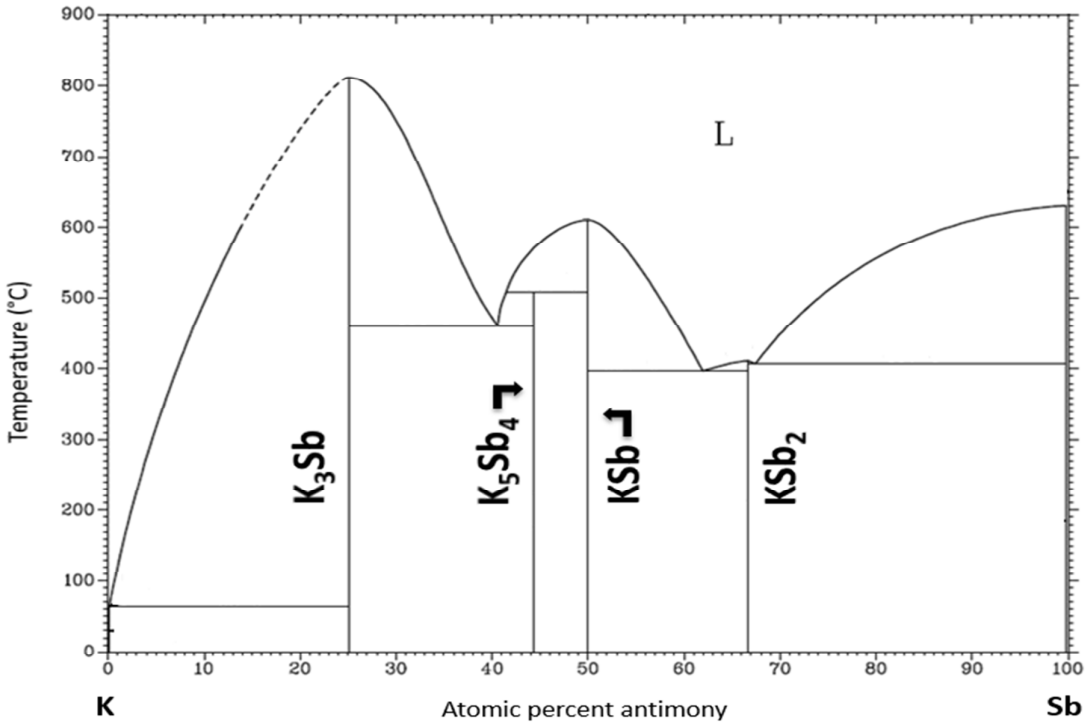

Figure S3. K-Sb phase diagram adapted from [1]

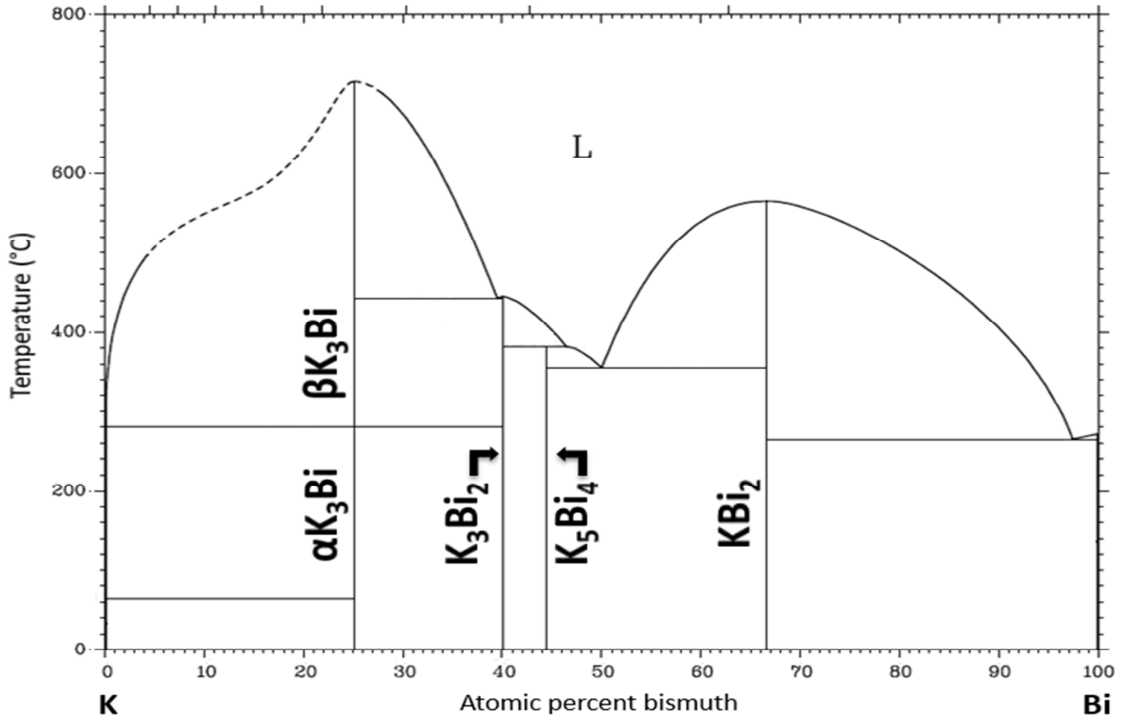

Figure S4. K-Bi phase diagram adapted from [2]

Evaluation of capacity from C65 carbon additive

It is well known that the theoretical capacity of carbon based electrode depends on the nature of carbon material [3]. In our case, the theoretical capacity of graphite (278 mAh/g) cannot be used for the C65 carbon black, since this material is mainly a disordered form of carbon. In order to estimate the effective capacity of such a carbon matrix, galvanostatic measurements were performed at C/26 rate on a C65/CMC (wt. % 70/30) electrode which showed a practical capacity of 260 mAh/g for the first discharge, and a reversible capacity of 156 mAh/g. The C65 electrode shows a sustainable capacity of 130 mAh/g for 50 cycles with a coulombic efficiency higher than 99 %. Considering that Sb or Bi electrodes contain 18 wt. % of C65, the contribution of carbon to the reversible capacity of the composite can be evaluated to 23.5 mAh/g.

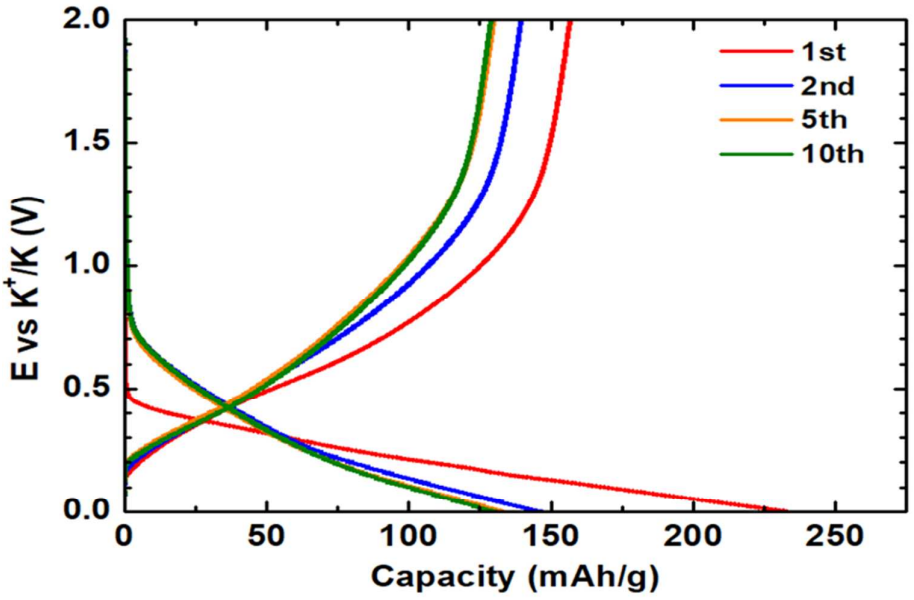

Figure S5. Galvanostatic discharge/charge curve of C65/CMC electrode at C/26 rate between 0.0 V and 2.0 V

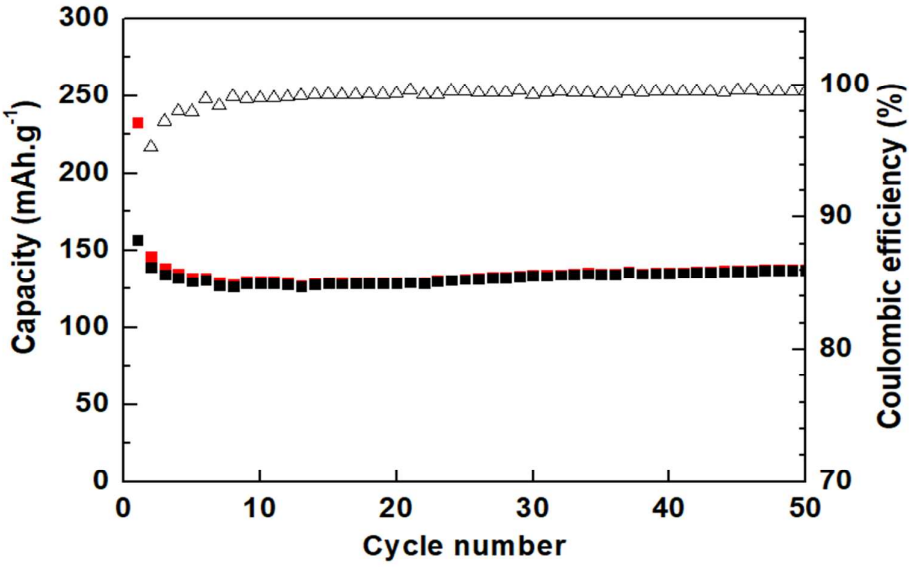

Figure S6. Capacity and coulombic efficiency of C65 electrode at C/26 rate plotted versus cycle number

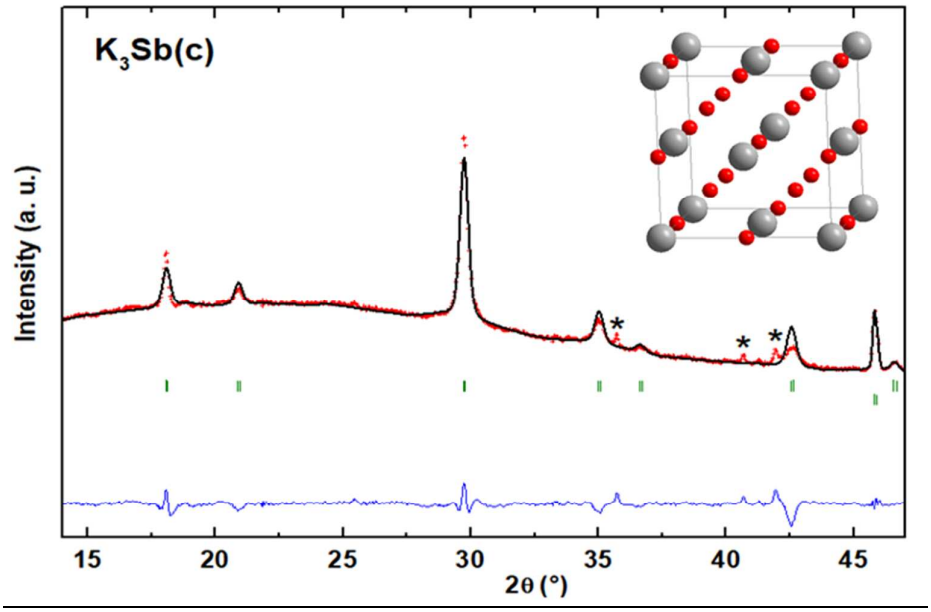

Figure S7. XRD *operando* pattern recorded for Sb electrode at the end of the first discharge

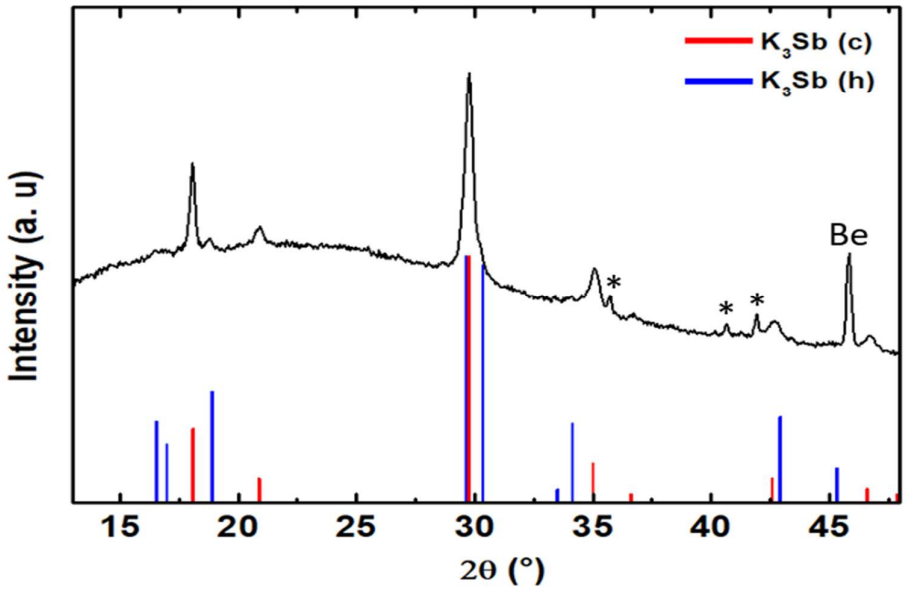

Figure S8. XRD *operando* pattern recorded for Sb electrode at the end of the first discharge

Synthesis of reference K_3Sb

For K_3Sb, both polymorphs are obtained at ambient conditions: the hexagonal polymorph is obtained by conventional high temperature synthesis, whereas cubic K_3Sb is formed in thin films by reducing oxidized Sb film.[4] A synthesis of K_3Sb by ball milling a stoichiometric mixture of Sb and K in argon shows a time dependence of the nature of the obtained polymorph (Fig. S9): the two polymorphs are obtained together after 200 min, while the relative amount of the cubic phase increase with milling time, and the cubic form is obtained after milling for 600 min. Such observation does not really clarify which of the two forms is the sable one at room temperature.

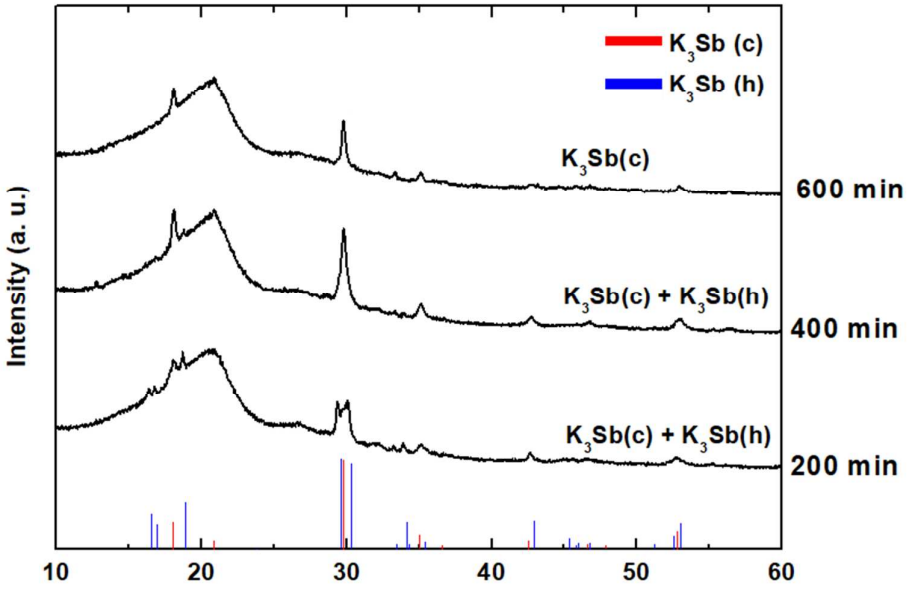

Figure S9. Evolution of XRD pattern of K_3Sb as a function of ball milling time

	Sb	Bi	Ref
1st Discharge vs Li	$^{c}Sb \rightarrow {}^{c}Li_2Sb \rightarrow {}^{c}Li_3Sb$	$^{c}Bi \rightarrow {}^{c}LiBi \rightarrow {}^{c}Li_3Bi$	[5-6]
1st Charge vs Li	$^{c}Li_3Sb \rightarrow {}^{c}Sb$	$^{c}Li_3Bi \rightarrow {}^{c}LiBi \rightarrow {}^{c}Bi$	
1st Discharge vs Na	$^{c}Sb \rightarrow {}^{a}Na_{3-x}Sb + {}^{c}Na_3Sb \rightarrow {}^{c}Na_3Sb$	$^{c}Bi \rightarrow {}^{c}NaBi \rightarrow {}^{c}Na_3Bi$	[7-8]
1st Charge vs Na	$^{c}Na_3Sb \rightarrow {}^{a}Na_{1.7}Sb \rightarrow {}^{a}NaSb \rightarrow {}^{c}Sb + {}^{a}NaSb$	$^{c}Na_3Bi \rightarrow {}^{c}NaBi \rightarrow {}^{c}Bi$	
1st Discharge vs K	**$^{c}Sb \rightarrow {}^{a}K_xSb \rightarrow {}^{c}K_3Sb$**	**$^{c}Bi \rightarrow {}^{c}K_3Bi$**	**This work**
1st Charge vs K	**$^{c}K_3Sb \rightarrow {}^{a}K_xSb \rightarrow {}^{a}Sb$**	**$^{c}K_3Bi \rightarrow {}^{c}K_3Bi_2 \rightarrow {}^{c}KBi_2 \rightarrow {}^{c}Bi$**	

Table S10. Summary of the electrochemical alkalinisation of Sb and Bi electrodes

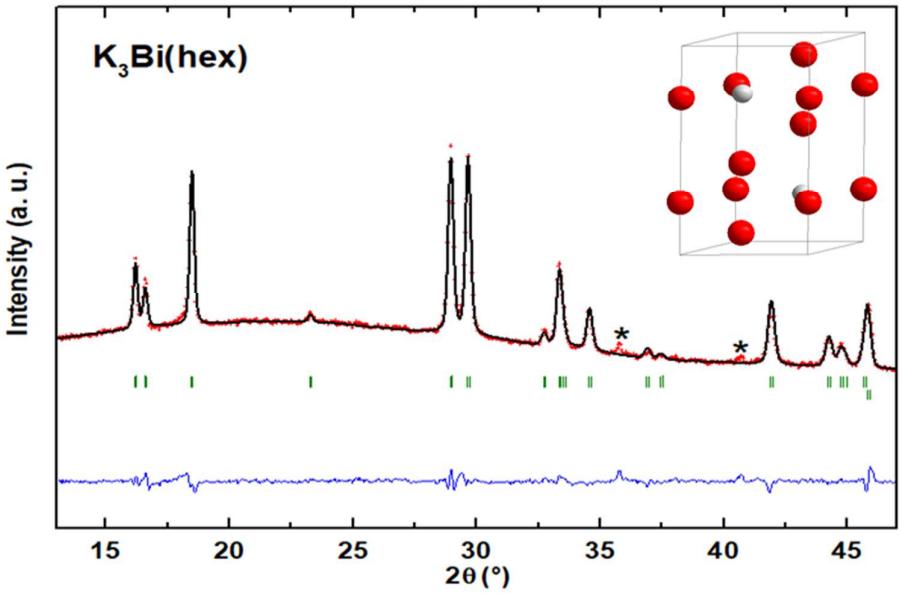

Figure S11. XRD *operando* pattern recorded for Bi electrode at the end of the first discharge

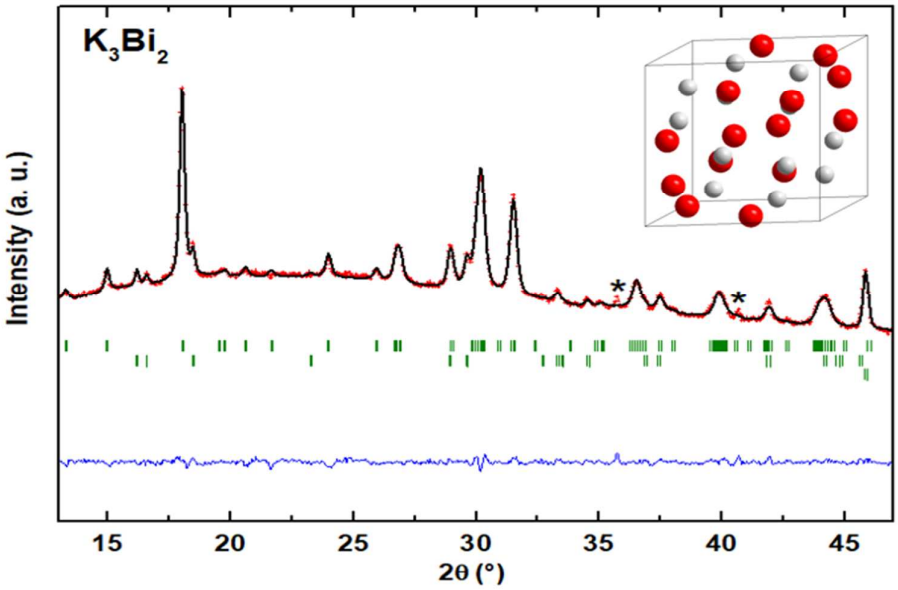

Figure S12. XRD *operando* pattern recorded for Bi electrode at 0.55 V during the first charge

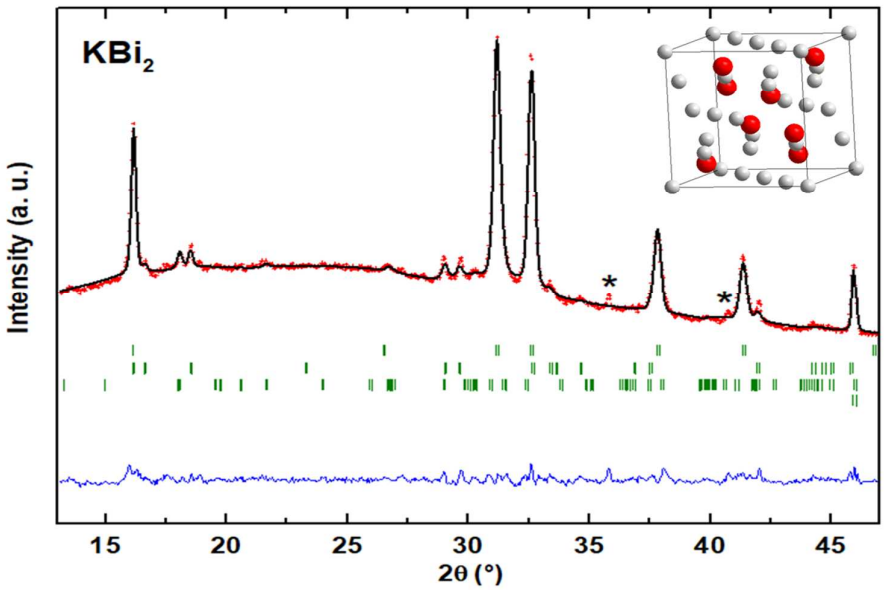

Figure S13. XRD *operando* pattern recorded for Bi electrode at 0.7 V during the first charge

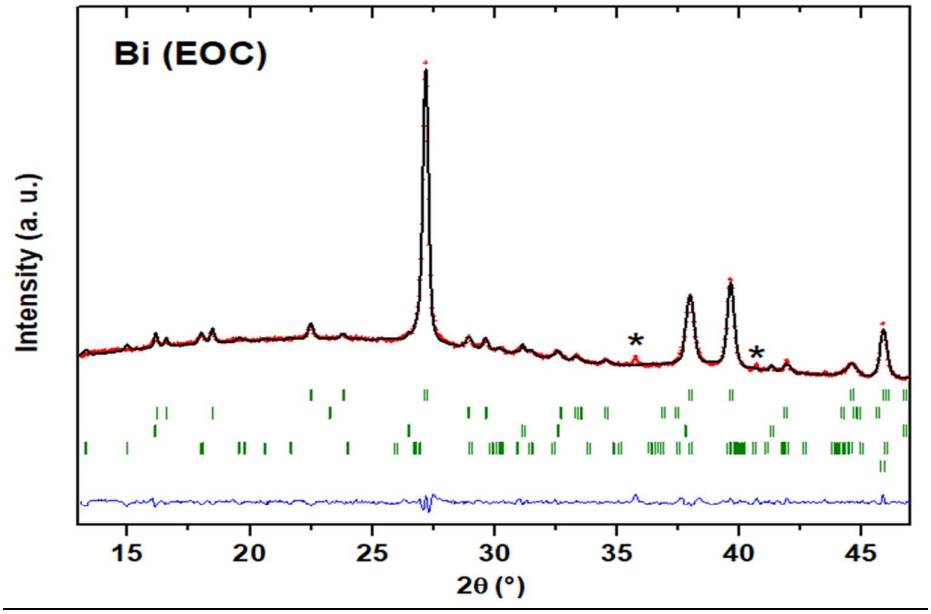

Figure S14. XRD *operando* pattern recorded for Bi electrode at 1.5 V, end of the first charge

In situ XRD phases	Space group	a (Å)	b (Å)	c (Å)	α	β	γ	References
K_3Sb(cubic)	*F m -3 m*	8.496(1)	8.496(1)	8.496(1)	90	90	90	This work
		8.493	8.493	8.493	90	90	90	00-019-0935
K_3Bi(hexagonal)	*P 63/m m c*	6.167(1)	6.167(1)	10943(1)	90	90	120	This work
		6.178	6.178	10.933	90	90	120	01-074-1165
K_3Bi_2	*C 2/c*	9.403(1)	9.817(1)	9.298(1)	90	105.04(1)	90	This work
		9.381	9.794	9.284	90	104.99	90	[9]
KBi_2	*F d -3m*	9.512(1)	9.512(1)	9.512(1)	90	90	90	This work
		9.52	9.52	9.52	90	90	90	00-003-0698
Bi (EOC)	*R -3 m*	4.547	4..547	11.861	90	90	120	This work
		4.546	4.546	11.862	90	90	120	01-085-1329

Table S15. Crystal structure parameters for the phases observed during the discharge/charge of Sb and Bi electrodes

		Cycle 1				Cycle 5			Cycle 10			Cycle 25		
		Discharge capacity (mAh/g)	Charge capacity (mAh/g)	Irreversible capacity (mAh/g)	CE (%)	Discharge capacity (mAh/g)	Charge capacity (mAh/g)	CE (%)	Discharge capacity (mAh/g)	Charge capacity (mAh/g)	CE (%)	Discharge capacity (mAh/g)	Charge capacity (mAh/g)	CE (%)
C65	**Capacity of carbon**	232.7	156.6	76.1	67.3	132.3	129.6	98.0	130.0	128.6	99.0	131.7	131.0	99.0
Sb	**Capacity calculated on the mass of active material + carbon**	746.9	626.7	120.2	83.9	613.3	604.1	98.5	604.7	592.2	97.9	308.9	254.3	82.3
Sb/C		569.6	387.9	181.7	68.1	398.5	391.2	98.2	399.3	394.8	98.9	379.9	371.1	97.7
Bi		426.4	345.3	81.1	80.9	323.7	259.8	80.3	246.5	232.6	94.3	227.3	220.6	97.0
Sb	**Capacity calculated on the mass of active material only**	938.9	787.8	151.1	83.9	771.0	759.4	98.5	760.2	744.5	97.9	388.4	319.7	82.3
Sb/C		1139.3	775.8	363.5	68.1	796.9	782.4	98.2	798.6	789.7	98.9	759.9	742.1	97.7
Bi		536.1	434.1	102.0	80.9	406.9	326.6	80.3	309.9	292.4	94.3	285.8	277.3	97.0

Table S16. Summary of gravimetric capacities for each electrode taking into account the mass of carbon or not

REFERENCES

(1) J. Sangster, A.D. Pelton, The K-Sb (Potassium-Antimony) system, *J. Phase Equilibria*. **1993**, 14, 510–514.

(2) Petric, A, Pelton, A. . The Bi-K (Bismuth-Potassium) System. *J. Phase Equilibria* **1991**, *12* (1), 29–33

(3) J.R. Dahn, T. Zheng, Y. Liu, J.S. Xue, Mechanisms for Lithium Insertion in Carbonaceous Materials, *Science*. **1995**, 270, 590–593.

(4) A.H. Sommer, W.H. McCarroll, A New Modification of the Semiconducting Compound K3Sb, *J. Appl. Phys*. **1966**, 37, 174–179.

(5) D. Chang, H. Huo, K.E. Johnston, M. Ménétrier, L. Monconduit, C.P. Grey, A. Van der Ven, Elucidating the origins of phase transformation hysteresis during electrochemical cycling of Li–Sb electrodes, *J. Mater. Chem. A*. **2015**, 3, 18928–18943.

(6) C.-M. Park, S. Yoon, S.-I. Lee, H.-J. Sohn, Enhanced electrochemical properties of nanostructured bismuth-based composites for rechargeable lithium batteries, *J. Power Sources*. **2009**, 186, 206–210.

(7) P.K. Allan, J.M. Griffin, A. Darwiche, O.J. Borkiewicz, K.M. Wiaderek, K.W. Chapman, A.J. Morris, P.J. Chupas, L. Monconduit, C.P. Grey, Tracking Sodium-Antimonide Phase Transformations in Sodium-Ion Anodes: Insights from Operando Pair Distribution Function Analysis and Solid-State NMR Spectroscopy, *J. Am. Chem. Soc*. **2016**, 138, 2352–2365.

(8) C. Wang, L. Wang, F. Li, F. Cheng, J. Chen, Bulk Bismuth as a High-Capacity and Ultralong Cycle-Life Anode for Sodium-Ion Batteries by Coupling with Glyme-Based Electrolytes, *Adv. Mater*. **2017**, 1702212.

(9) F. Gascoin, S.C. Sevov, Synthesis and characterization of A3Bi2 (A = K, Rb, Cs) with isolated diatomic dianion of bismuth, [Bi2]2-, and an extra delocalized electron, *J. Am. Chem. Soc.* **2002**, 122, 10251–10252.